Letter

Friction-mediated phase transition in confined active nematics

Cody D. Schimming,* C. J. O. Reichhardt, and C. Reichhardt
Theoretical Division and Center for Nonlinear Studies, Los Alamos National Laboratory, Los Alamos, New Mexico 87545, USA

(Received 28 February 2023; accepted 28 June 2023; published 27 July 2023)

Using a minimal continuum model, we investigate the interplay between circular confinement and substrate friction in active nematics. Upon increasing the friction from low to high, we observe a dynamical phase transition from a circulating flow phase to an anisotropic flow phase in which the flow tends to align perpendicular to the nematic director at the boundary. We demonstrate that both the flow structure and dynamic correlations in the latter phase differ from those of an unconfined, active turbulent system and may be controlled by the prescribed nematic boundary conditions. Our results show that substrate friction and geometric confinement act as valuable control parameters in active nematics.

DOI: 10.1103/PhysRevE.108.L012602

A remarkable feature of active fluids is their ability to generate macroscopic flows from energy consumption at the microscale [1,2]. In many cases, however, these flows are chaotic, a phenomenon dubbed "active turbulence" due to its qualitative similarities to inertial turbulence [3–12]. Identifying methods to control the flows generated by active fluids has recently been of particular interest due to potential technical and biomedical applications. Efforts in this direction have included coupling to concentration gradients, patterning activity, manipulating sample geometry, and imposing boundary conditions [13–23]. Here, we focus on "active nematics," active fluids composed of elongated constituents that produce macroscopic flows via force dipoles, and study the flow patterns that emerge from the interplay between two important and relevant control mechanisms: circular confinement [16,18,24–31] and substrate friction [32–38]. While the effects of these control mechanisms on the dynamical behavior of active nematics have been previously studied independently, their interplay still needs to be explored. Energy dissipation through frictional damping introduces a length scale, the hydrodynamic screening length, which sets the scale below which hydrodynamic interactions are important. Further, because nematics are inherently anisotropic, confinement allows the prescription of topologically and geometrically distinct boundary conditions. While it is known that the boundary conditions do not alter the flow state for frictionless systems [28], it is not known whether a paradigm exists in which the boundary conditions can tune the system dynamics.

Here, using a minimal continuum model, we show that when the hydrodynamic screening length is decreased, circularly confined active nematics transition from a circulating flow state to a dynamical anisotropic flow phase that, to our knowledge, has yet to be described. We show that the anisotropic flow phase is distinct from active turbulence, and is characterized by flows and vortices that organize perpendicular to the nematic boundary condition. As a result, the boundary conditions may be used to tune the dynamics and correlation timescales of the system. To investigate the interplay between confinement and hydrodynamic screening, we vary the screening length at a fixed average timescale associated with active stress injection [39]. This differs from previous investigations of the effects of substrate friction on bulk active nematics in which only the timescale associated with viscous forces is fixed, while the timescale associated with frictional damping is increased leading to the suppression of flow [32,33,37,40]. We find that the anisotropic flow transition occurs when the elastic interactions between defects become dominant due to the hydrodynamic screening length dropping below the size of the topological defects. Our results not only shed light on how biological systems, which tend to have larger screening lengths, organize flow and dynamics, but also can be used to engineer controlled flow and dynamics by employing hydrodynamic screening and boundary conditions as control parameters.

The numerical model we use has been previously well documented [41,42]. We briefly review it here and give specific details in the Supplemental Material [43]. The equations for the active nematic are written in terms of the nematic tensor order parameter $\mathbf{Q}$, the fluid velocity $\mathbf{v}$, and the fluid pressure p:.

$$\frac{\partial \mathbf{Q}}{\partial t} + (\mathbf{v}\cdot\nabla)\mathbf{Q} - \mathbf{S} = -\frac{1}{\gamma}\frac{\delta F}{\delta \mathbf{Q}}, \tag{1}$$

$$-\eta\nabla^2\mathbf{v} + \Gamma\mathbf{v} = -\nabla p - \alpha\nabla\cdot\mathbf{Q}, \quad \nabla\cdot\mathbf{v} = \mathbf{0}. \tag{2}$$

Equation (1) describes the time evolution of the nematic tensor order parameter $\mathbf{Q} = S[\mathbf{n}\otimes\mathbf{n} - (1/2)\mathbf{I}]$ where S gives the local degree of order and $\mathbf{n}$ is the nematic director. $\mathbf{S} = \mathbf{S}(\mathbf{Q}, \nabla\mathbf{v})$ is a generalized tensor advection [44], F is the usual Landau–de Gennes free energy in which we assume one-constant elasticity [45], and γ is a rotational viscosity. Equation (2) is the modified Stokes equation describing low Reynolds number flows. Here, η is the fluid viscosity. The terms proportional to Γ and α are additions to the usual Stokes equation and they describe, respectively, friction

*cschim@lanl.gov

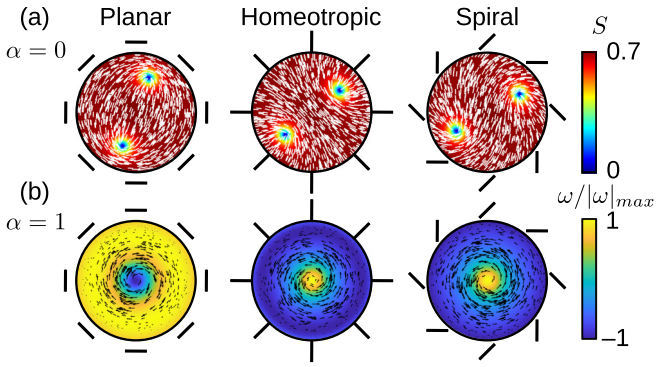

FIG. 1. (a) Nonactive ($\alpha = 0$) nematic configurations for the three boundary conditions studied: planar, homeotropic, and spiral anchoring. The color in the plots shows the local scalar order parameter S while the white lines show the nematic director $\mathbf{n}$. Lines outside the domain depict the fixed orientation of the nematic director at the boundary. (b) Example velocity and vorticity fields for simulated active ($\alpha = 1$) nematics with $L_{SC} = 10$. The color shows the normalized vorticity field, while the arrows show the magnitude and direction of the velocity.

between the active nematic and substrate and the strength of active forces in the nematic [42]. $\alpha > 0$ corresponds to extensile forces while $\alpha < 0$ corresponds to contractile forces. The divergence-free condition on the velocity models an incompressible fluid. A discussion of the length scales and timescales associated with the model is given in the Supplemental Material [43].

We nondimensionalize, discretize, and solve Eqs. (1) and (2) numerically on a circular domain using fixed nematic boundary conditions with the MATLAB/C++ finite-element package FELICITY [46]. We fix the domain radius to $\tilde{R} = 7.5$ in dimensionless units (see Supplemental Material [43] for details on dimensionless quantities). We also fix the ratio $\tilde{\alpha}/(\tilde{\eta} + \tilde{\Gamma}) = 1$ and vary only the hydrodynamic screening length $\tilde{L}_{SC} = \sqrt{\tilde{\eta}/\tilde{\Gamma}}$. The tildes denote dimensionless quantities and are omitted in what follows for brevity. This procedure differs from previous explorations of the effect of friction on bulk active nematics in that we do not hold the viscosity constant [32,33,36,37,40]. As detailed in the Supplemental Material, constraining the ratio $\alpha/(\eta + \Gamma) = 1$ fixes the average active timescale associated with viscous and frictional forces and yields a dimensionless Stokes equation in which the active force is relevant across all scales of the hydrodynamic screening length. This allows us to isolate the effect of the screening length without suppressing the flows generated by the active stress [43]. We choose $\alpha/(\eta + \Gamma) = 1$ since this leads to the circulation phase in the zero friction limit for our chosen domain size [28]. Much smaller values lead to a quiescent state, while much larger values lead to turbulent behavior.

We consider three nematic boundary conditions: planar, homeotropic, and spiral. Figure 1(a) shows the nonactive ($\alpha = 0$) state for each of these boundary conditions. All three boundary conditions impose an overall topological charge of $+1$ on the system, so topological defects (points of singular nematic orientation, called disclinations) must form. In the nonactive state, the lowest-energy configuration consists of two $+1/2$ winding number disclinations that lie on opposite ends of the domain. In active nematics, $+1/2$ disclinations are motile, and so the configurations we consider show dynamical behavior at lower activities than bulk systems with zero overall topological charge [42].

For the active system ($\alpha = 1$), varying L_{SC} induces a clear transition between two distinct dynamical phases. For large L_{SC} (low friction) the long-time dynamical behavior of the system is characterized by circulating flow. For small L_{SC} (high friction), the circulation ceases and a dynamical anisotropic flow phase reminiscent of active turbulence emerges. Unlike traditional active turbulence, the anisotropic flow is characterized by long, thin vortices that organize near the boundary to lie perpendicular to the nematic director.

The circulation phase observed at large L_{SC} is depicted in Fig. 1(b), where we plot the velocity and vorticity fields for the three boundary conditions at $L_{SC} = 10$. In all cases, a central vortex is formed and the flow circulates in a clockwise or counterclockwise direction. For the level of activity we consider, the nematic configuration initially contains two $+1/2$ defects circulating each other at early times that eventually merge, causing the configuration to develop a central $+1$ defect with a spiral pattern for all boundary conditions (Fig. S1).

The direction of circulation is a spontaneously broken symmetry for planar and homeotropic anchoring, since these boundary conditions are achiral; however, the spiral boundary conditions break chiral symmetry and always produce counterclockwise flow. If the boundary conditions were rotated by $\pi/2$, the resulting flow would circulate in the opposite direction. Hence, the spiral boundary condition offers a method of controlling the direction of flow, similar to that shown in experiments with bacterial suspensions in a prepatterned liquid crystal [17] except that it is not necessary to prepattern the entire liquid crystal, but only the director at the boundary of the sample.

In contrast, the dynamics of the anisotropic flow phase at small L_{SC} depend on the choice of nematic boundary condition. Figures 2(a) and 2(b) show time snapshots of the nematic configuration and velocity and vorticity fields for each boundary condition at $L_{SC} = 0.2$. The many long, thin vortices in this phase tend to lie perpendicular to the fixed nematic director at the boundary, and as a result, the flow direction is influenced by the prescribed boundary conditions.

While the anisotropic flow phase is qualitatively reminiscent of traditional active turbulence, we show in Fig. 2(c) that the time-averaged velocity and vorticity fields retain structure when averaged over the length of the simulation. This differs from the zero flow time average obtained in a chaotic, turbulent system, as seen in simulations of unconfined active nematics with periodic boundary conditions (Fig. S2). As shown in Fig. 2(c), for both planar and homeotropic boundary conditions we find persistent organization of vortices near the boundary. The spiral boundary conditions produce time-averaged circulating flow near the boundary instead of the distinct spiral vortex pattern found in the time snapshot of Fig. 2(b). This is because the dynamics of the vortices are relatively static for planar and homeotropic boundary conditions, but circulate for spiral conditions as a result of the promotion of circulating flows (see Supplemental Movies 1–3).

The primary mechanism behind the perpendicular alignment of the flow field to the nematic director at the boundary

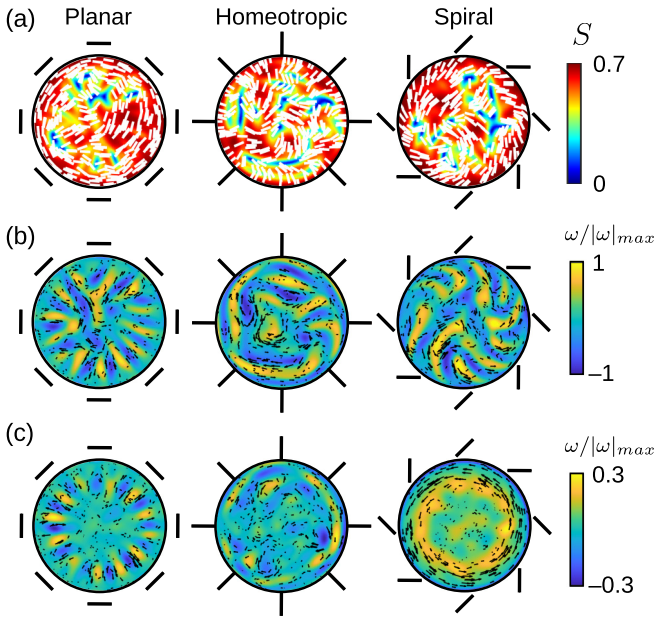

FIG. 2. (a) Time snapshots of the nematic configurations for simulated active nematics with $L_{SC} = 0.2$. (b) Velocity and vorticity fields at same time snapshot as in (a). (c) Time-averaged velocity and vorticity fields for the same simulations.

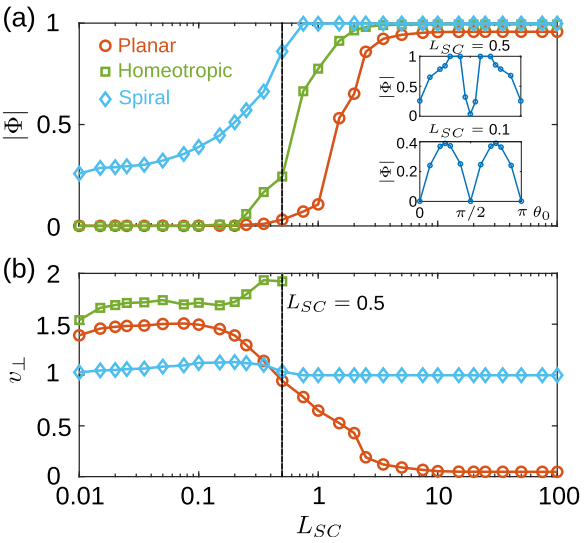

FIG. 3. (a) Flow circulation $|\Phi|$ vs hydrodynamic screening length L_{SC} for confined active nematic systems with planar, homeotropic, and spiral anchoring. Inset: $|\Phi|$ vs anchoring angle θ_0 for $L_{SC} = 0.5$ and $L_{SC} = 0.1$. (b) Perpendicular flow parameter $v_\perp$ vs L_{SC}. The dashed line in both plots marks $L_{SC} = 0.5$, below which the confined system is in the anisotropic flow phase.

is the active nematic bend instability [47], which promotes undulations in the nematic director that form parallel to the director. Since L_{SC} controls the size of vortices [32], it also controls the size of the undulations. When L_{SC} is small enough, the undulations become large enough to support the unbinding of $\pm 1/2$ disclination pairs that generate flows perpendicular to the director. Thus, the nematic configuration in the anisotropic flow phase is characterized by motile $+1/2$ disclinations unbinding near the boundary and then, at a later time, annihilating with immotile $-1/2$ disclinations that remain near the boundary (see Supplemental Movies 1–3).

To quantitatively describe the system, we define two parameters related to the velocity of the fluid. The circulation parameter is [29]

$$\Phi = \left\langle \frac{v_\theta}{|\mathbf{v}|} \right\rangle, \tag{3}$$

where v_θ is the azimuthal component of the velocity. All averages are computed over the full simulation time and spatial domain. For coherent circular flows, $\Phi = \pm 1$, while for chaotic, active turbulent flows, $\Phi = 0$. We also measure the average ratio of flow perpendicular to the nematic director boundary condition $\mathbf{n}_0$ to that parallel to $\mathbf{n}_0$:

$$v_\perp = \left\langle \frac{|\mathbf{v} \times \mathbf{n}_0|}{|\mathbf{v} \cdot \mathbf{n}_0|} \right\rangle. \tag{4}$$

We note that this perpendicular flow measure depends on the boundary condition. For a chaotic, active turbulent state we expect $v_\perp = 1$, that is, an equal proportion of perpendicular and parallel flows.

Figure 3 shows $|\Phi|$ and $v_\perp$ vs L_{SC} for systems with hydrodynamic screening ranging over several orders of magnitude. For planar and homeotropic anchoring, the circulation parameter $|\Phi|$ ranges from 1 at large L_{SC} to 0 at small L_{SC}. The spiral boundary conditions always have nonzero circulation, but $|\Phi|$ decreases as L_{SC} is reduced. We also measured $|\Phi|$ for systems with anchoring angle $\theta_0 \in [0, \pi]$ with respect to the boundary and $L_{SC} = 0.5$ and $L_{SC} = 0.1$, as shown in the inset of Fig. 3(a). We find that in the anisotropic flow phase ($L_{SC} = 0.1$) the maximal circulation occurs for spiral anchoring, $\theta_0 = \pi/4, 3\pi/4$. However, near the phase transition ($L_{SC} = 0.5$) the circulation is maximal close to planar anchoring, $\theta_0 = \pi/2$, before dropping to zero exactly at planar anchoring. In this case, the circulating phase is stabilized by the shear flow resulting from the central vortex shown in Fig. 1(b). The nematic tends to align at an angle relative to the flow, the "Leslie angle," which for our system is close to planar anchoring [43,48]. Thus, if θ_0 is close to the Leslie angle, the circulating phase will remain stable for a larger range of L_{SC}. This indicates that the transition itself may be tunable by material parameters that control the flow alignment.

While $|\Phi|$ serves as an order parameter that indicates a transition between dynamical phases, the perpendicular flow parameter $v_\perp$ quantifies the nature of the anisotropic flow phase at small L_{SC}. Since $v_\perp$ depends on the director $\mathbf{n}_0$ at the boundary, its definition changes for different boundary conditions. For example, for planar boundary conditions we obtain $v_\perp = \langle |v_r|/|v_\theta| \rangle$, where v_r is the radial component of the velocity, while for homeotropic boundary conditions we obtain the reciprocal, $v_\perp = \langle |v_\theta|/|v_r| \rangle$. For coherent circulating flows, then, $v_\perp$ goes to zero for planar boundary conditions but diverges for homeotropic boundary conditions. Remarkably, in the anisotropic flow phase $v_\perp$ is very similar for the planar and homeotropic cases, even though $v_\perp$ is defined reciprocally. We mark the transition to anisotropic flow in Fig. 3 as occurring at $L_{SC} = 0.5$, since below this value, $v_\perp > 1$ for the three considered boundary conditions.

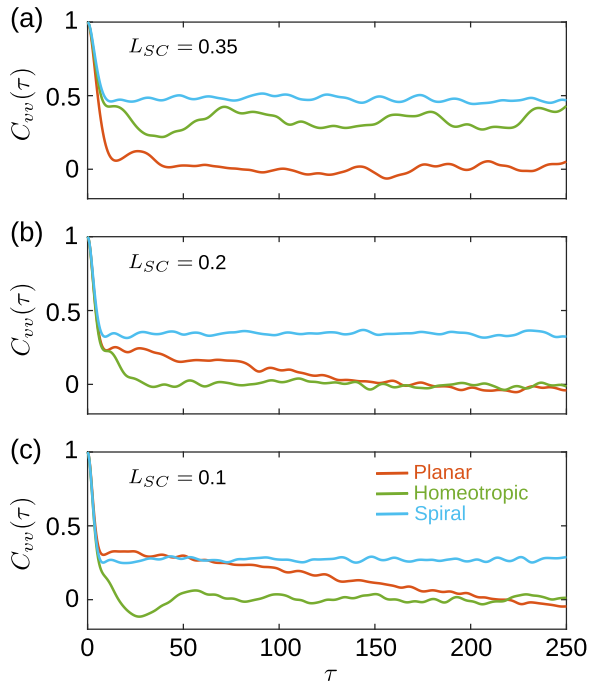

FIG. 4. Velocity time correlation function $C_{vv}(\tau)$ plotted for simulations with hydrodynamic screening lengths (a) $L_{SC} = 0.35$, (b) $L_{SC} = 0.2$, and (c) $L_{SC} = 0.1$ for planar, homeotropic, and spiral anchoring.

For our choice of model parameters [43], $L_{SC} = 0.5$ is roughly the radius of the topological defects, suggesting that the hydrodynamic interaction between defects promotes circulation, and that the transition to anisotropic flow occurs when elastic interactions (i.e., Coulomb-like interactions) between defects become dominant.

To better understand the dynamics of the anisotropic flow phase, in Fig. 4 we plot the velocity time correlation function

$$C_{vv}(\tau) = \left\langle \frac{\mathbf{v}(t+\tau)\cdot\mathbf{v}(t)}{|\mathbf{v}(t)|^2} \right\rangle \tag{5}$$

for simulations with $L_{SC} = 0.35$, $L_{SC} = 0.2$, and $L_{SC} = 0.1$. Interestingly, the dynamics differ depending on the boundary condition. Due to the overall circulation, the flows for spiral boundary conditions remain correlated for long times even as L_{SC} is decreased. Near the transition ($L_{SC} = 0.35$), however, we find that homeotropic boundary conditions give correlated flows due to the residual circulation present in the system, while planar boundary conditions result in uncorrelated flows. As L_{SC} decreases, systems with homeotropic boundary conditions become uncorrelated, while systems with planar anchoring become more correlated and require longer times to become uncorrelated. Additionally, the velocity correlation functions in the confined system are markedly different from those observed in unconfined systems, which exhibit completely uncorrelated flows at small L_{SC} (Fig. S3).

The differences between the dynamics for planar and homeotropic boundary conditions can be explained by the average structure of the flows shown in Fig. 2(b). For planar anchoring, the vortices on average form an azimuthal periodic structure around the boundary, while for homeotropic anchoring, all periodicity is destroyed as L_{SC} diminishes and the vortices become smaller. These results suggest that both the structure and dynamics of the anisotropic flow phase may be tuned with the nematic boundary condition, which gives insight into how biological systems organize flows and has implications for technological applications of active fluids involving controlled mixing.

Summary. In this Letter, using the hydrodynamic screening length as a control parameter, we show that circularly confined active nematics transition with decreasing screening length from a circulating flow phase to an anisotropic flow phase characterized by flow organized perpendicularly to the nematic boundary condition. Both dynamical phases feature organized flows distinct from those found in the well-known active turbulent phase. Our work shows that substrate friction and confinement can be used as control mechanisms for the directionality and dynamic correlations of flows via the nematic boundary conditions. While there has been some experimental work in which the substrate is altered such that an effective friction is varied [20,25], the interplay between confinement and friction still needs to be explored experimentally. Following the results of Ref. [20], we propose that the depth of the oil layer may be varied in a circularly confined microtubule-based active nematic in order to reproduce our results experimentally. It has additionally been shown both experimentally and numerically that similar transitions occur in three-dimensional active nematics as the system becomes more confined [27,49,50]. This indicates that three-dimensional confinement may act as an effective friction on the system and that the complex flows observed may potentially be explained by the simpler two-dimensional model used here.

Future work includes expanding the phase diagram for confined active nematics. In this study we have only varied the screening length L_{SC}, but we expect a rich dynamical phase landscape to emerge as the activity is also varied. This would lead to a better understanding of the interplay between the screening length, the nematic correlation length, and the active length. Additionally, different types of confinement may yield even more modes of control over active systems. We explored the effect of positive curvature, but negative curvature could be induced by a circular inclusion. Experiments in annuli have already shown controlled circulating behavior [16,27] and immersed microstructures have been shown to pin defects [23]. Due to the increasing degree of experimental and engineered control over boundary geometries and confinement, the understanding of how active fluids interact with their environment is becoming more important and practical.

This work was supported by the U.S. Department of Energy through the Los Alamos National Laboratory. Los Alamos National Laboratory is operated by Triad National Security, LLC, for the National Nuclear Security Administration of the U.S. Department of Energy (Contract No. 89233218CNA000001).

[1] S. Ramaswamy, The mechanics and statistics of active matter, Annu. Rev. Condens. Matter Phys. **1**, 323 (2010).

[2] M. C. Marchetti, J. F. Joanny, S. Ramaswamy, T. B. Liverpool, J. Prost, M. Rao, and R. A. Simha, Hydrodynamics of soft active matter, Rev. Mod. Phys. **85**, 1143 (2013).

[3] H. H. Wensink, J. Dunkel, S. Heidenreich, K. Drescher, R. E. Goldstein, H. Löwen, and J. M. Yeomans, Meso-scale turbulence in living fluids, Proc. Natl. Acad. Sci. USA **109**, 14308 (2012).

[4] T. Sanchez, D. T. N. Chen, S. J. DeCamp, M. Heymann, and Z. Dogic, Spontaneous motion in hierarchically assembled active matter, Nature (London) **491**, 431 (2012).

[5] A. Creppy, O. Praud, X. Druart, P. L. Kohnke, and F. Plouraboué, Turbulence of swarming sperm, Phys. Rev. E **92**, 032722 (2015).

[6] D. Nishiguchi and M. Sano, Mesoscopic turbulence and local order in Janus particles self-propelling under an ac electric field, Phys. Rev. E **92**, 052309 (2015).

[7] T. D. Yang, H. Kim, C. Yoon, S.-K. Baek, and K. J. Lee, Collective pulsatile expansion and swirls in proliferating tumor tissue, New J. Phys. **18**, 103032 (2016).

[8] M. M. Genkin, A. Sokolov, O. D. Lavrentovich, and I. S. Aranson, Topological Defects in a Living Nematic Ensnare Swimming Bacteria, Phys. Rev. X **7**, 011029 (2017).

[9] A. Doostmohammadi, T. N. Shendruk, K. Thijssen, and J. M. Yeomans, Onset of meso-scale turbulence in active nematics, Nat. Commun. **8**, 15326 (2017).

[10] R. Alert, J.-F. Joanny, and J. Casademunt, Universal scaling of active nematic turbulence, Nat. Phys. **16**, 682 (2020).

[11] L. N. Carenza, L. Biferale, and G. Gonnella, Cascade or not cascade? Energy transfer and elastic effects in active nematics, Europhys. Lett. **132**, 44003 (2020).

[12] R. Alert, J. Casademunt, and J.-F. Joanny, Active turbulence, Annu. Rev. Condens. Matter Phys. **13**, 143 (2022).

[13] P. Guillamat, J. Ignés-Mullol, and F. Sagués, Control of active liquid crystals with a magnetic field, Proc. Natl. Acad. Sci. USA **113**, 5498 (2016).

[14] S. Zhou, O. Tovkach, D. Golovaty, A. Sokolov, I. S. Aranson, and O. D. Lavrentovich, Dynamic states of swimming bacteria in a nematic liquid crystal cell with homeotropic alignment, New J. Phys. **19**, 055006 (2017).

[15] A. Sokolov, A. Mozaffari, R. Zhang, J. J. de Pablo, and A. Snezhko, Emergence of Radial Tree of Bend Stripes in Active Nematics, Phys. Rev. X **9**, 031014 (2019).

[16] J. Hardoüin, J. Laurent, T. Lopez-Leon, J. Ignés-Mullol, and F. Sagués, Active microfluidic transport in two-dimensional handlebodies, Soft Matter **16**, 9230 (2020).

[17] R. Koizumi, T. Turiv, M. M. Genkin, R. J. Lastowski, H. Yu, I. Chaganava, Q.-H. Wei, I. S. Aranson, and O. D. Lavrentovich, Control of microswimmers by spiral nematic vortices: Transition from individual to collective motion and contraction, expansion, and stable circulation of bacterial swirls, Phys. Rev. Res. **2**, 033060 (2020).

[18] M. M. Norton, P. Grover, M. F. Hagan, and S. Fraden, Optimal Control of Active Nematics, Phys. Rev. Lett. **125**, 178005 (2020).

[19] C. Reichhardt and C. J. O. Reichhardt, Directional locking effects for active matter particles coupled to a periodic substrate, Phys. Rev. E **102**, 042616 (2020).

[20] K. Thijssen, D. A. Khaladj, S. A. Aghvami, M. A. Gharbi, S. Fraden, J. M. Yeomans, L. S. Hirst, and T. N. Shendruk, Submersed micropatterned structures control active nematic flow, topology, and concentration, Proc. Natl. Acad. Sci. USA **118**, e2106038118 (2021).

[21] P. M. Vinze, A. Choudhary, and S. Pushpavanam, Motion of an active particle in a linear concentration gradient, Phys. Fluids **33**, 032011 (2021).

[22] R. Zhang, S. A. Redford, P. V. Ruijgrok, N. Kumar, A. Mozaffari, S. Zemsky, A. R. Dinner, V. Vitelli, Z. Bryant, M. L. Gardel, and J. J. de Pablo, Spatiotemporal control of liquid crystal structure and dynamics through activity patterning, Nat. Mater. **20**, 875 (2021).

[23] N. Figueroa-Morales, M. M. Genkin, A. Sokolov, and I. S. Aranson, Non-symmetric pinning of topological defects in living liquid crystals, Commun. Phys. **5**, 301 (2022).

[24] H. Wioland, F. G. Woodhouse, J. Dunkel, J. O. Kessler, and R. E. Goldstein, Confinement Stabilizes a Bacterial Suspension into a Spiral Vortex, Phys. Rev. Lett. **110**, 268102 (2013).

[25] P. Guillamat, J. Ignés-Mullol, S. Shankar, M. C. Marchetti, and F. Sagués, Probing the shear viscosity of an active nematic film, Phys. Rev. E **94**, 060602(R) (2016).

[26] M. Theillard, R. Alonso-Matilla, and D. Saintillan, Geometric control of active collective motion, Soft Matter **13**, 363 (2017).

[27] K.-T. Wu, J. B. Hishamunda, D. T. N. Chen, S. J. DeCamp, Y.-W. Chang, A. Fernández-Nieves, S. Fraden, and Z. Dogic, Transition from turbulent to coherent flows in confined three-dimensional active fluids, Science **355**, eaal1979 (2017).

[28] M. M. Norton, A. Baskaran, A. Opathalage, B. Langeslay, S. Fraden, A. Baskaran, and M. F. Hagan, Insensitivity of active nematic liquid crystal dynamics to topological constraints, Phys. Rev. E **97**, 012702 (2018).

[29] A. Opathalage, M. M. Norton, M. P. N. Juniper, B. Langeslay, S. A. Aghvami, S. Fraden, and Z. Dogic, Self-organized dynamics and the transition to turbulence of confined active nematics, Proc. Natl. Acad. Sci. USA **116**, 4788 (2019).

[30] A. Mozaffari, R. Zhang, N. Atzin, and J. J. de Pablo, Defect Spirograph: Dynamical Behavior of Defects in Spatially Patterned Active Nematics, Phys. Rev. Lett. **126**, 227801 (2021).

[31] P. Guillamat, C. Blanch-Mercader, G. Pernollet, K. Kruse, and A. Roux, Integer topological defects organize stresses driving tissue morphogenesis, Nat. Mater. **21**, 588 (2022).

[32] A. Doostmohammadi, M. F. Adamer, S. P. Thampi, and J. M. Yeomans, Stabilization of active matter by flow-vortex lattices and defect ordering, Nat. Commun. **7**, 10557 (2016).

[33] A. Doostmohammadi, S. P. Thampi, and J. M. Yeomans, Defect-Mediated Morphologies in Growing Cell Colonies, Phys. Rev. Lett. **117**, 048102 (2016).

[34] E. Putzig, G. S. Redner, A. Baskaran, and A. Baskaran, Instabilities, defects, and defect ordering in an overdamped active nematic, Soft Matter **12**, 3854 (2016).

[35] P. Srivastava, P. Mishra, and M. C. Marchetti, Negative stiffness and modulated states in active nematics, Soft Matter **12**, 8214 (2016).

[36] A. Doostmohammadi and J. M. Yeomans, Coherent motion of dense active matter, Eur. Phys. J. Spec. Top. **227**, 2401 (2019).

[37] K. Thijssen, L. Metselaar, J. M. Yeomans, and A. Doostmohammadi, Active nematics with anisotropic friction: the decisive role of the flow aligning parameter, Soft Matter **16**, 2065 (2020).

[38] K. Thijssen, M. R. Nejad, and J. M. Yeomans, Role of Friction in Multidefect Ordering, Phys. Rev. Lett. **125**, 218004 (2020).

[39] L. Giomi, M. J. Bowick, P. Mishra, R. Sknepnek, and M. Cristina Marchetti, Defect dynamics in active nematics, Philos. Trans. R. Soc. A **372**, 20130365 (2014).

[40] S. P. Thampi, R. Golestanian, and J. M. Yeomans, Active nematic materials with substrate friction, Phys. Rev. E **90**, 062307 (2014).

[41] D. Marenduzzo, E. Orlandini, M. E. Cates, and J. M. Yeomans, Steady-state hydrodynamic instabilities of active liquid crystals: Hybrid lattice Boltzmann simulations, Phys. Rev. E **76**, 031921 (2007).

[42] A. Doostmohammadi, J. Ignés-Mullol, J. M. Yeomans, and F. Sagués, Active nematics, Nat. Commun. **9**, 3246 (2018).

[43] See Supplemental Material at http://link.aps.org/supplemental/10.1103/PhysRevE.108.L012602 for details on the continuum model, numerical method, unconfined active nematic simulations, and supplemental figures and videos.

[44] A. N. Beris and B. J. Edwards, *Thermodynamics of Flowing Systems* (Oxford University Press, Oxford, UK, 1994).

[45] P. G. de Gennes, *The Physics of Liquid Crystals* (Oxford University Press, Oxford, UK, 1975).

[46] S. W. Walker, FELICITY: A MATLAB/C++ toolbox for developing finite element methods and simulation modeling, SIAM J. Sci. Comput. **40**, C234 (2018).

[47] S. Ramaswamy and M. Rao, Active-filament hydrodynamics: instabilities, boundary conditions and rheology, New J. Phys. **9**, 423 (2007).

[48] F. M. Leslie, Continuum theory for nematic liquid crystals, Continuum Mech. Thermodyn. **4**, 167 (1992).

[49] S. Chandragiri, A. Doostmohammadi, J. M. Yeomans, and S. P. Thampi, Flow States and Transitions of an Active Nematic in a Three-Dimensional Channel, Phys. Rev. Lett. **125**, 148002 (2020).

[50] M. Varghese, A. Baskaran, M. F. Hagan, and A. Baskaran, Confinement-Induced Self-Pumping in 3D Active Fluids, Phys. Rev. Lett. **125**, 268003 (2020).